Scour in Long Contractions

Subhasish Dey[1] and Rajkumar V. Raikar[2]

Abstract: Experimental results on local scour in long contractions for uniform and nonuniform sediments (gravels and sands) under clear-water scour are presented. An emphasis was given to conduct the experiments on scour in long contractions for gravels. The findings of the experiments are used to describe the effects of various parameters (obtained from dimensional analysis) on equilibrium scour depth under clear-water scour. The equilibrium scour depth increases with decrease in opening ratio and with increase in sediment size for gravels. But the curves of scour depth versus sediment size have considerable sag at the transition of sand and gravel. The scour depth decreases with increase in densimetric Froude number, for larger opening ratios, and increases with increase in approaching flow depth at lower depths. However, it becomes independent of approaching flow depth at higher flow depths. The effect of sediment gradation on scour depth is pronounced for nonuniform sediments, which reduce scour depth significantly due to the formation of armor layer in the scour hole. Using the continuity and energy equations, a simple analytical model for the computation of clear-water scour depth in long contractions is developed with and without sidewall correction for contracted zone. The models agree satisfactorily with the present and other experimental data. Also, a new empirical equation of maximum equilibrium scour depth, which is based on the experimental data at the limiting stability of sediments in approaching channel under clear-water scour, is proposed. The potential predictors of the maximum equilibrium scour depth in long contractions are compared with the experimental data. The comparisons indicate that the equations given by Komura and Lim are the best predictors among those examined.

DOI: 10.1061/(ASCE)0733-9429(2005)131:12(1036)

CE Database subject headings: Open channel flow; Nonuniform flow; Steady flow; Contraction; Erosion; Scour; Sediment transport.

Introduction

A reduction of width of a watercourse by constructing parallel sidewalls is termed channel contraction. Contractions of river width to construct bridges, barrages, weirs, and cross-drainage works are common examples of channel contractions. Also, partial closure required for the maintenance of channel riverbanks, such as construction of cofferdam and end-dump channel constriction, is the other type of channel contraction. Depending on the ratio of the length of contraction L to the approaching channel width b_1, channel contractions are designated as long or short (see the schematic of a rectangular contraction given in Fig. 1). According to Komura (1966), a contraction becomes long when $L/b_1 > 1$, whereas Webby (1984) considered it as $L/b_1 > 2$. However, recent experimental investigation of Raikar (2004), who measured the flow field by the acoustic Doppler velocimeter (ADV) in channel contractions, confirmed that $L/b_1 \geq 1$ is adequate for a contraction to be considered long, as the velocity distribution including turbulence characteristics (turbulent kinetic energy) in the contracted region remains unchanged almost over the entire length of contraction (Figs. 2 and 3).

The flow velocity in the contracted zone of the channel increases due to the reduction of flow area, and hence the bed shear stress induced by the flow increases considerably. Consequently, the sediment bed within the channel contraction is scoured. Such localized scour in the contracted zone of the channel is called contraction scour. Based on the supply of sediment by the approaching flow, the localized scour is classified as clear-water scour and live-bed scour (Dey 1997). Clear-water scour occurs when sediment is removed from the scour hole but not supplied by the approaching flow; whereas live-bed scour occurs when there is a general sediment transport by the approaching flow. Local scour in a channel contraction is usually studied considering a configuration of rectangular long contraction, as shown schematically in Fig. 1. Because of the simple geometrical configuration of the problem, various analytical investigations to predict the maximum scour depth in long contractions have been attempted. Straub (1934) was the pioneer to present a simplified one-dimensional theory of the equilibrium scour in long contractions. His work was later extended and modified by Ashida (1963), Laursen (1963), Komura (1966), Gill (1981), and Webby (1984). Lim (1993) proposed an empirical equation of maximum equilibrium scour depth in long contractions under clear-water and live-bed scour conditions. From the aforementioned studies, it is revealed that a detailed investigation describing the effects of various parameters on scour depth in long contractions is inadequate. Also, little attention is paid to study the scour depth of gravel-bed in long contractions.

The present study aims at a detailed parametric investigation on scour depth in long contractions for uniform and nonuniform sediments (gravels and sands) under clear-water scour. The findings of the experimental investigation are used to describe the

[1]Associate Professor, Dept. of Civil Engineering, Indian Institute of Technology, Kharagpur 721302, West Bengal, India. Email: sdey@iitkgp.ac.in

[2]Doctoral Research Fellow, Dept. of Civil Engineering, Indian Institute of Technology, Kharagpur 721302, West Bengal, India. Email: raikar@civil.iitkgp.ernet.in

Note. Discussion open until May 1, 2006. Separate discussions must be submitted for individual papers. To extend the closing date by one month, a written request must be filed with the ASCE Managing Editor. The manuscript for this paper was submitted for review and possible publication on January 8, 2004; approved on February 11, 2005. This paper is part of the ***Journal of Hydraulic Engineering***, Vol. 131, No. 12, December 1, 2005. ©ASCE, ISSN 0733-9429/2005/12-1036–1049/ $25.00.

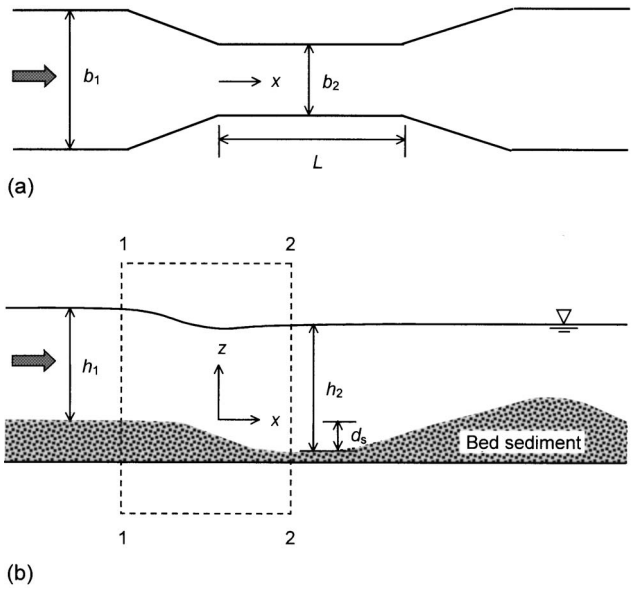

Fig. 1. Schematic of a long rectangular channel contraction at equilibrium scour condition: (a) top view; and (b) side view

effects of various parameters on scour depth, to determine a new equation of maximum equilibrium scour depth empirically and to compare the potential predictors of maximum equilibrium scour depth. Also, based on the continuity and energy equations, a simple analytical model for computation of clear-water scour depth in long contractions is developed with and without sidewall correction.

Experimental Setup and Procedure

The laboratory experiments were carried out in a 12 m long, 0.6 m wide, and 0.7 m deep tilting flume at the Hydraulic and Water Resources Engineering Laboratory, Indian Institute of Technology, Kharagpur. The contraction models were prepared by 12-mm-thick perspex sheets having uniform contraction zone of 1 m length. The upstream and downstream transitions of the contraction model were made smooth, providing the angles of upstream transition 13° [slightly greater than 12.5° for a smooth transition (Smith 1967)] and downstream transition 15°. Fig. 1 shows the schematic view of a long rectangular channel contraction. Contraction models for four opening ratios $\tilde{b}$ ($=b_2/b_1$) of 0.7, 0.6, 0.5, and 0.4 were used in this study; where b_2 is the width of the contracted zone. The models were symmetrically attached to the side glass walls of the flume in a sediment recess of 3 m long, 0.6 m wide, and 0.3 m deep, containing sediments. The upstream end of the contraction model was located at 6 m from the flume inlet in order to have a fully developed turbulent flow at the entrance of the contraction. The flow discharge, controlled by an inlet valve, was measured using a calibrated rectangular weir fitted at the outflow channel, where the water from the flume was discharged. The flow depth in the flume was adjusted by a downstream tailgate. A Vernier point gauge with an accuracy of ±0.1 mm was used to measure the flow depths. To avoid the undesirable scour, which would otherwise happen by the action of sheet flow with inadequate flow depth, the flume was initially filled with water issued from a pipe at a low rate until the desirable flow depth was reached. Then the discharge in the flume was

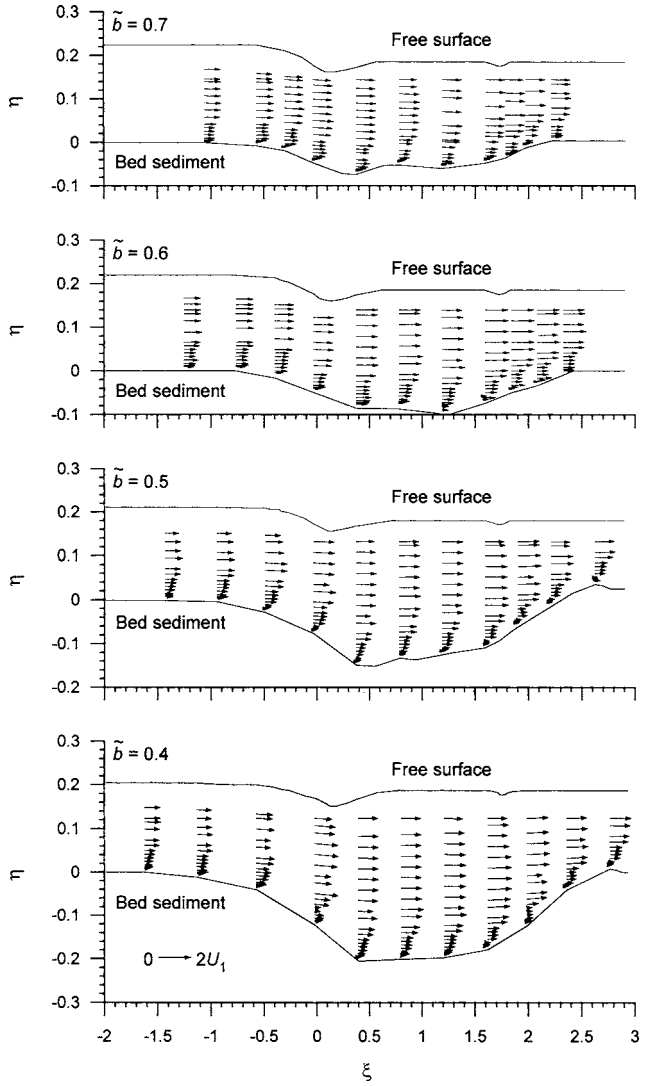

Fig. 2. Normalized velocity vectors along the centerline for $\tilde{b}$=0.7, 0.6, 0.5, and 0.4

gradually increased to the desired value corresponding to the clear-water scour condition, and the experiment was run till the equilibrium scour reached. For the scouring tests, three sand sizes and five gravel sizes were used. As inadequate attention has so far been paid on scour of gravel bed in long contractions, an emphasis is given to study the scour in contractions for different sizes of gravels. The properties of the uniform sediments used in the experiments are given in Table 1. The degree of uniformity of the particle size distribution of a sediment sample is defined by the value of geometric standard deviation σ_g, given by $(d_{84}/d_{16})^{0.5}$, which is less than 1.4 for uniform sediments (Dey et al. 1995). Two different sets of experimental data were collected (Tables 2 and 3). In the first set (Table 2), experiments were run with uniform sediments for the average approaching flow velocities $0.98U_c > U_1 > 0.9U_c$ being achieved by adjusting the discharge and tailgate, where U_c=critical velocity for sediments. On the other hand, in the second set (Table 3), experiments were run with nonuniform sediments ($\sigma_g > 1.4$) for $0.98 > U_1/U_c > 0.9$ and $\tilde{b}$=0.6. Therefore, the experiments were conducted under a clear-water scour condition, maintaining $U_1/U_c < 1$ or $u_{*1}/u_{*c} < 1$; where u_{*1} is the approaching shear velocity; and u_{*c} is the critical shear velocity for sediments. The approaching shear velocity u_{*1}

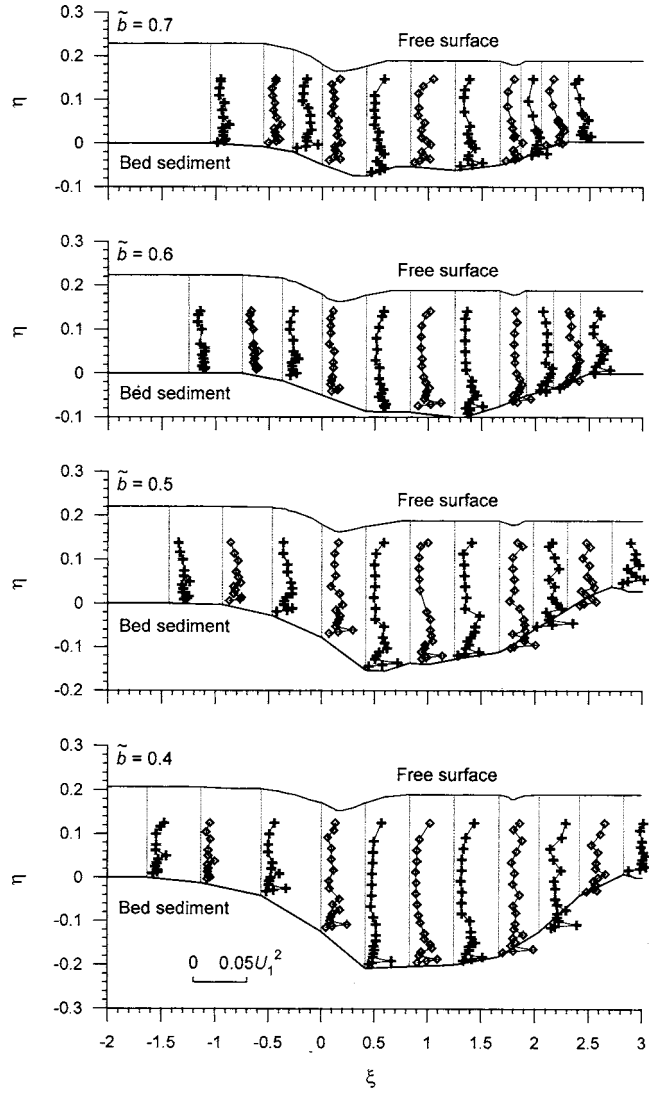

Fig. 3. Vertical distribution of normalized turbulent kinetic energy $\hat{k}$ along the centerline for $\tilde{b}$=0.7, 0.6, 0.5, and 0.4

is obtained from the semilogarithmic plot of the approaching flow velocity distribution measured at the midsection of the flume located at 0.5 m upstream of the entrance of the channel contraction, where the free approaching flow prevailed. The critical shear velocities u_{*c} for sediments furnished in Table 1 were obtained from the Shields diagram. The corresponding critical velocities U_c were calculated using the semilogarithmic average velocity equation for a rough bed, as was done by Lauchlan and Melville (2001). The equation of semilogarithmic average velocity is

$$\frac{U_c}{u_{*c}} = 5.75 \log\frac{h_1}{2d_{50}} + 6 \quad (1)$$

where h_1=approaching flow depth and d_{50}=median sediment diameter.

Gill (1981) indicated that the equilibrium scour depth in long channel contractions becomes maximum when $U_1/U_c \rightarrow 1$ under clear-water scour. But, it is important to mention that the approaching channel bed becomes disturbed by the approaching flow at the critical condition of sediment motion, that is $U_1 \rightarrow U_c$. This prompted to run the experiments for $0.98 > U_1/U_c > 0.9$, in which the approaching channel beds remained undisturbed. The scour data of first set are used to analyze the effects of different parameters on scour depth and to determine the equation of maximum equilibrium scour depth. On the other hand, the effect of nonuniform sediments on scour depth is analyzed using the data of the second set. The experiments were run under clear-water scour conditions for a period of more than 24 h until an equilibrium state of scour was achieved, which was ascertained when a negligible (1 mm or nil) difference of scour depth was observed at an interval of 2 h after 24 h. Then, the flow discharge was slowly reduced to zero, and the water was carefully drained out from the scoured zone of sediment recess. A Vernier point gauge was used to measure the scour depths and free surface profiles. In this study, the equilibrium scour depths d_s were observed near the centerline within the contracted zone. The bed sediment size, width of approaching channel, width of contracted zone, approaching flow velocity, approaching flow depth, geometric standard deviation of sediments, and scour depth for different runs are furnished in Tables 2 and 3. Figs. 4(a and b) show the photographs of scour within channel contraction.

Table 1. Characteristics of Sediments Used in the Experiments

Type	Median diameter d_{50} (mm)	Relative density s	Geometric standard deviation σ_g	Angle of repose ϕ (deg)	Critical shear velocity u_{*c} (m/s)
Sand	0.81	2.65	1.342	30	0.0202
	1.86	2.65	1.270	30.5	0.0347
	2.54	2.65	1.065	31	0.0423
Gravel	4.10	2.65	1.130	32.5	0.0546
	5.53	2.65	1.100	34	0.0635
	7.15	2.65	1.080	35	0.0715
	10.25	2.65	1.160	37	0.0864
	14.25	2.65	1.090	39	0.1019

The instantaneous three-dimensional velocity components and turbulence were measured by a SonTek (San Diego) made 5 cm downlooking ADV. The ADV operated on a pulse-to-pulse coherent Doppler shift to provide instantaneous three-dimensional velocity components at a rate of 50 Hz. The main intension of the flow field measurement by ADV was to have an understanding on the characteristics of velocity and turbulence distributions. Fig. 2 exhibits the normalized time-averaged velocity vectors along the centerline of the channel before and after the contraction plotted on a nondimensional plane $\xi\eta$, where $\xi = x/b_1$ and $\eta = y/b_1$. The velocity vectors inside the scour hole show that the flow field is considerably similar within the contraction. The turbulence characteristics can be examined from the distributions of the normalized turbulent kinetic energy $\hat{k}$ [$=k/U_1^2$ where k=turbulent kinetic energy] along the centerline of the channel as shown in Fig. 3. The bulges in the distribution of $\hat{k}$ near the bed in the scour hole indicate that the turbulent fluctuation is significant near the bed resulting from bed roughness due to gravels. Nevertheless, there was a considerable similarity in the distribution of $\hat{k}$ within the contraction.

Influences of Various Parameters on Scour Depth

Dimensional Analysis

The parameters influencing the equilibrium scour depth d_s in a long contraction can be given in a functional form as follows:

Table 2. Experimental Data for Uniform Sediments under Clear-Water Scour

d_{50} (mm)	U_1 (m/s)	U_1/U_c	h_1 (m)	b_1 (m)	b_2 (m)	Observed d_s (m)	Computed with sidewall correction d_s (m)	Computed without sidewall correction d_s (m)
Sediment type: Sand								
0.81	0.311	0.965	0.0870	0.60	0.42	0.026	0.033	0.029
0.81	0.327	0.963	0.1230	0.60	0.42	0.039	0.048	0.040
0.81	0.313	0.975	0.0854	0.60	0.36	0.029	0.051	0.046
0.81	0.332	0.972	0.1280	0.60	0.36	0.056	0.081	0.068
0.81	0.311	0.954	0.0940	0.60	0.30	0.072	0.083	0.072
0.81	0.323	0.949	0.1250	0.60	0.30	0.095	0.114	0.096
0.81	0.314	0.964	0.0937	0.60	0.24	0.090	0.129	0.110
0.81	0.332	0.970	0.1300	0.60	0.24	0.149	0.188	0.155
1.86	0.467	0.959	0.0930	0.60	0.42	0.027	0.033	0.031
1.86	0.491	0.954	0.1280	0.60	0.42	0.045	0.046	0.041
1.86	0.468	0.957	0.0950	0.60	0.36	0.063	0.053	0.049
1.86	0.492	0.953	0.1300	0.60	0.36	0.078	0.074	0.067
1.86	0.475	0.968	0.0970	0.60	0.30	0.096	0.084	0.077
1.86	0.491	0.954	0.1280	0.60	0.30	0.108	0.112	0.099
1.86	0.473	0.966	0.0960	0.60	0.24	0.143	0.126	0.113
1.86	0.491	0.955	0.1270	0.60	0.24	0.154	0.170	0.147
2.54	0.531	0.943	0.0950	0.60	0.42	0.025	0.032	0.031
2.54	0.561	0.944	0.1273	0.60	0.42	0.038	0.044	0.041
2.54	0.544	0.957	0.1000	0.60	0.36	0.054	0.056	0.052
2.54	0.567	0.956	0.1260	0.60	0.36	0.064	0.071	0.066
2.54	0.535	0.952	0.0940	0.60	0.30	0.088	0.078	0.073
2.54	0.562	0.946	0.1270	0.60	0.30	0.092	0.108	0.098
2.54	0.534	0.947	0.0955	0.60	0.24	0.110	0.120	0.110
2.54	0.568	0.954	0.1286	0.60	0.24	0.139	0.169	0.149
Sediment type: Gravel								
4.10	0.602	0.960	0.0738	0.60	0.42	0.030	0.026	0.026
4.10	0.633	0.960	0.0935	0.60	0.42	0.036	0.033	0.032
4.10	0.622	0.928	0.1010	0.60	0.42	0.040	0.033	0.032
4.10	0.657	0.923	0.1373	0.60	0.42	0.041	0.045	0.042
4.10	0.596	0.942	0.0768	0.60	0.36	0.043	0.041	0.041
4.10	0.614	0.950	0.0849	0.60	0.36	0.056	0.046	0.045
4.10	0.631	0.923	0.1115	0.60	0.36	0.059	0.058	0.056
4.10	0.658	0.925	0.1366	0.60	0.36	0.065	0.072	0.068
4.10	0.576	0.931	0.0692	0.60	0.30	0.069	0.055	0.054
4.10	0.618	0.946	0.0892	0.60	0.30	0.079	0.073	0.070
4.10	0.612	0.913	0.1010	0.60	0.30	0.083	0.079	0.075
4.10	0.641	0.907	0.1322	0.60	0.30	0.097	0.104	0.096
4.10	0.592	0.934	0.0772	0.60	0.24	0.079	0.093	0.089
4.10	0.610	0.932	0.0903	0.60	0.24	0.092	0.109	0.103
4.10	0.626	0.925	0.1063	0.60	0.24	0.129	0.129	0.119
4.10	0.659	0.944	0.1242	0.60	0.24	0.131	0.157	0.143
5.53	0.630	0.927	0.0726	0.60	0.42	0.022	0.024	0.025
5.53	0.689	0.976	0.0859	0.60	0.42	0.037	0.031	0.031
5.53	0.690	0.936	0.1048	0.60	0.42	0.041	0.035	0.035
5.53	0.716	0.940	0.1220	0.60	0.42	0.044	0.041	0.040
5.53	0.647	0.958	0.0707	0.60	0.36	0.051	0.039	0.039
5.53	0.668	0.940	0.0886	0.60	0.36	0.063	0.048	0.047
5.53	0.696	0.938	0.1077	0.60	0.36	0.070	0.058	0.056
5.53	0.713	0.929	0.1269	0.60	0.36	0.069	0.067	0.065

Table 2. (*Continued.*)

d_{50} (mm)	U_1 (m/s)	U_1/U_c	h_1 (m)	b_1 (m)	b_2 (m)	Observed d_s (m)	Computed with sidewall correction d_s (m)	Computed without sidewall correction d_s (m)
5.53	0.644	0.953	0.0710	0.60	0.30	0.068	0.058	0.058
5.53	0.664	0.933	0.0891	0.60	0.30	0.080	0.071	0.070
5.53	0.673	0.907	0.1079	0.60	0.30	0.089	0.084	0.080
5.53	0.709	0.922	0.1277	0.60	0.30	0.099	0.102	0.097
5.53	0.639	0.944	0.0716	0.60	0.24	0.074	0.087	0.084
5.53	0.660	0.941	0.0835	0.60	0.24	0.098	0.101	0.097
5.53	0.671	0.906	0.1070	0.60	0.24	0.103	0.126	0.118
5.53	0.704	0.915	0.1281	0.60	0.24	0.133	0.155	0.142
7.15	0.701	0.956	0.0786	0.60	0.42	0.034	0.028	0.028
7.15	0.711	0.956	0.0833	0.60	0.42	0.039	0.030	0.030
7.15	0.715	0.914	0.1036	0.60	0.42	0.041	0.034	0.034
7.15	0.747	0.917	0.1240	0.60	0.42	0.044	0.040	0.040
7.15	0.676	0.957	0.0677	0.60	0.36	0.052	0.038	0.038
7.15	0.691	0.923	0.0857	0.60	0.36	0.062	0.045	0.045
7.15	0.715	0.913	0.1037	0.60	0.36	0.062	0.054	0.053
7.15	0.760	0.936	0.1219	0.60	0.36	0.068	0.066	0.064
7.15	0.663	0.939	0.0675	0.60	0.30	0.071	0.055	0.055
7.15	0.688	0.930	0.0817	0.60	0.30	0.081	0.066	0.065
7.15	0.717	0.917	0.1033	0.60	0.30	0.093	0.081	0.079
7.15	0.754	0.927	0.1229	0.60	0.30	0.101	0.099	0.095
7.15	0.672	0.950	0.0681	0.60	0.24	0.079	0.083	0.082
7.15	0.711	0.951	0.0853	0.60	0.24	0.089	0.105	0.101
7.15	0.712	0.913	0.1020	0.60	0.24	0.103	0.121	0.115
7.15	0.753	0.926	0.1230	0.60	0.24	0.135	0.149	0.140
10.25	0.755	0.918	0.0840	0.60	0.42	0.029	0.029	0.030
10.25	0.777	0.901	0.1010	0.60	0.42	0.031	0.033	0.034
10.25	0.813	0.900	0.1220	0.60	0.42	0.049	0.040	0.040
10.25	0.746	0.921	0.0793	0.60	0.36	0.046	0.043	0.044
10.25	0.770	0.922	0.0890	0.60	0.36	0.055	0.048	0.049
10.25	0.778	0.902	0.1010	0.60	0.36	0.060	0.053	0.053
10.25	0.816	0.904	0.1215	0.60	0.36	0.069	0.063	0.063
10.25	0.769	0.957	0.0770	0.60	0.30	0.071	0.065	0.065
10.25	0.764	0.913	0.0897	0.60	0.30	0.073	0.072	0.071
10.25	0.783	0.906	0.1018	0.60	0.30	0.076	0.080	0.079
10.25	0.820	0.910	0.1210	0.60	0.30	0.104	0.096	0.093
10.25	0.749	0.925	0.0790	0.60	0.24	0.084	0.095	0.094
10.25	0.768	0.919	0.0892	0.60	0.24	0.087	0.107	0.104
10.25	0.825	0.944	0.1063	0.60	0.24	0.106	0.131	0.127
10.25	0.820	0.910	0.1210	0.60	0.24	0.138	0.144	0.138
14.25	0.832	0.923	0.0890	0.60	0.42	0.050	0.033	0.033
14.25	0.886	0.941	0.1045	0.60	0.42	0.052	0.038	0.039
14.25	0.929	0.947	0.1220	0.60	0.42	0.051	0.044	0.045
14.25	0.863	0.952	0.0910	0.60	0.36	0.061	0.053	0.053
14.25	0.891	0.947	0.1040	0.60	0.36	0.073	0.059	0.059
14.25	0.908	0.920	0.1247	0.60	0.36	0.074	0.068	0.068
14.25	0.842	0.937	0.0880	0.60	0.30	0.081	0.074	0.074
14.25	0.864	0.911	0.1072	0.60	0.30	0.091	0.087	0.086
14.25	0.929	0.947	0.1220	0.60	0.30	0.108	0.102	0.101
14.25	0.847	0.944	0.0875	0.60	0.24	0.110	0.109	0.107
14.25	0.858	0.903	0.1080	0.60	0.24	0.118	0.128	0.125
14.25	0.891	0.910	0.1210	0.60	0.24	0.144	0.145	0.140

Note: Ranges of tilting angles and lengths of upstream transition were 0–1.3 % and 0.4–0.8 m, respectively.

Table 3. Experimental Data for Nonuniform Sediments under Clear-Water Scour

d_{50} (mm)	σ_g	U_1 (m/s)	U_1/U_c	h_1 (m)	b_1 (m)	b_2 (m)	d_s (m)
Sediment type: Sand							
0.81	1.342	0.332	0.972	0.1280	0.60	0.36	0.056
0.81	1.800	0.332	0.972	0.1280	0.60	0.36	0.046
0.81	2.450	0.332	0.972	0.1280	0.60	0.36	0.021
0.81	3.130	0.332	0.972	0.1280	0.60	0.36	0.015
1.86	1.270	0.492	0.953	0.1300	0.60	0.36	0.065
1.86	1.850	0.492	0.953	0.1300	0.60	0.36	0.051
1.86	2.600	0.492	0.953	0.1300	0.60	0.36	0.021
1.86	3.160	0.492	0.953	0.1300	0.60	0.36	0.017
2.54	1.065	0.567	0.956	0.1260	0.60	0.36	0.064
2.54	1.960	0.567	0.956	0.1260	0.60	0.36	0.041
2.54	2.950	0.567	0.956	0.1260	0.60	0.36	0.018
2.54	3.600	0.567	0.956	0.1260	0.60	0.36	0.016
Sediment type: Gravel							
4.10	1.130	0.658	0.925	0.1366	0.60	0.36	0.065
4.10	1.505	0.658	0.925	0.1366	0.60	0.36	0.059
4.10	1.954	0.658	0.925	0.1366	0.60	0.36	0.029
4.10	2.673	0.658	0.925	0.1366	0.60	0.36	0.017
5.53	1.100	0.713	0.929	0.1269	0.60	0.36	0.069
5.53	1.433	0.713	0.929	0.1269	0.60	0.36	0.061
5.53	2.027	0.713	0.929	0.1269	0.60	0.36	0.025
5.53	2.321	0.713	0.929	0.1269	0.60	0.36	0.020
7.15	1.080	0.760	0.936	0.1219	0.60	0.36	0.068
7.15	1.514	0.760	0.936	0.1219	0.60	0.36	0.059
7.15	2.070	0.760	0.936	0.1219	0.60	0.36	0.026
7.15	2.928	0.760	0.936	0.1219	0.60	0.36	0.016
10.25	1.160	0.816	0.904	0.1215	0.60	0.36	0.069
10.25	1.496	0.816	0.904	0.1215	0.60	0.36	0.062
10.25	1.937	0.816	0.904	0.1215	0.60	0.36	0.031
10.25	2.513	0.816	0.904	0.1215	0.60	0.36	0.019
14.25	1.090	0.908	0.920	0.1247	0.60	0.36	0.074
14.25	1.464	0.908	0.920	0.1247	0.60	0.36	0.069
14.25	1.634	0.908	0.920	0.1247	0.60	0.36	0.057
14.25	1.826	0.908	0.920	0.1247	0.60	0.36	0.052

$$d_s = f_1(U_1, h_1, \rho, \rho_s, g, \nu, d_{50}, b_1, b_2, \sigma_g) \quad (2)$$

where ρ=mass density of water; ρ_s=mass density of sediments; g=gravitational acceleration; and ν=kinematic viscosity of water ($=10^{-6}$ m^2/s). In sediment–water interaction, it is appropriate to represent the independent parameters g, ρ, and ρ_s as a combined parameter Δg (Dey and Debnath 2001; Dey and Barbhuiya 2004a) ; where $\Delta = s-1$; and s=relative density of sediments, that is ρ_s/ρ. Also, from the point of view of physical reasoning, it is a logical choice to use the parameter channel opening ratio $\tilde{b}$ in order to have a combined effect of b_1 and b_2. In addition, the influence of kinematic viscosity ν is considered negligible under a fully turbulent flow over a rough bed (Yalin 1977). Applying the Buckingham π theorem with repeating variables U_1 and b_1, and rearranging the nondimensional parameters logically, yields

$$\tilde{d}_s = f_2(\tilde{d}, \mathsf{F}_0, \tilde{h}, \tilde{b}, \sigma_g) \quad (3)$$

where $\tilde{d}_s = d_s/b_1$; $\tilde{d} = d_{50}/b_1$; $\mathsf{F}_0 = U_1/(\Delta g d_{50})^{0.5}$, that is the densimetric Froude number; and $\tilde{h} = h_1/b_1$.

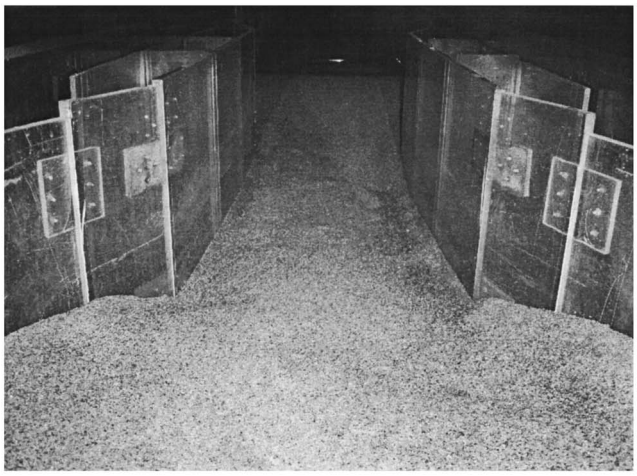

(a)

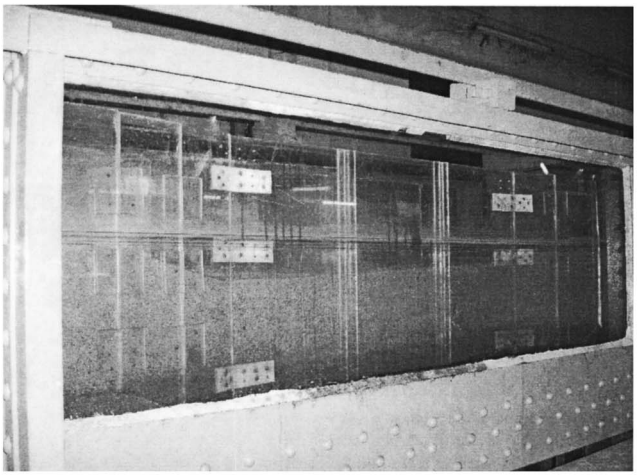

(b)

Fig. 4. Scour within channel contraction: (a) facing upstream and (b) side view of scoured bed

The justification of the effects of the nondimensional parameters on scour depth is as follows:

- The term $\tilde{d}$ indicates the influence of sediment size on scour depth;
- The term F_0 represents the effect of the mobility of submerged sediment particles on scour depth;
- The term $\tilde{h}$ indicates the role of approaching flow depth on scour depth;
- The term $\tilde{b}$ refers to the effect of degree of channel contraction on scour depth; and
- The term σ_g corresponds to the influence of the gradation of sediment particles on scour depth.

Dependency of Scour Depth on Various Parameters

The laboratory experimental data (Table 2) for four channel opening ratios $\tilde{b}$, tested for $\tilde{h}$=0.2–0.233 and d_{50}=0.81–14.25 mm under the approaching flow conditions of $0.972 > U_1/U_c > 0.9$, are used to plot nondimensional equilibrium scour depth $\tilde{d}_s$ versus $\tilde{d}$ in Fig. 6(a), which shows that $\tilde{d}_s$ increases almost linearly with increase in $\tilde{d}$ for gravels ($\tilde{d} > 0.0065$). For sands

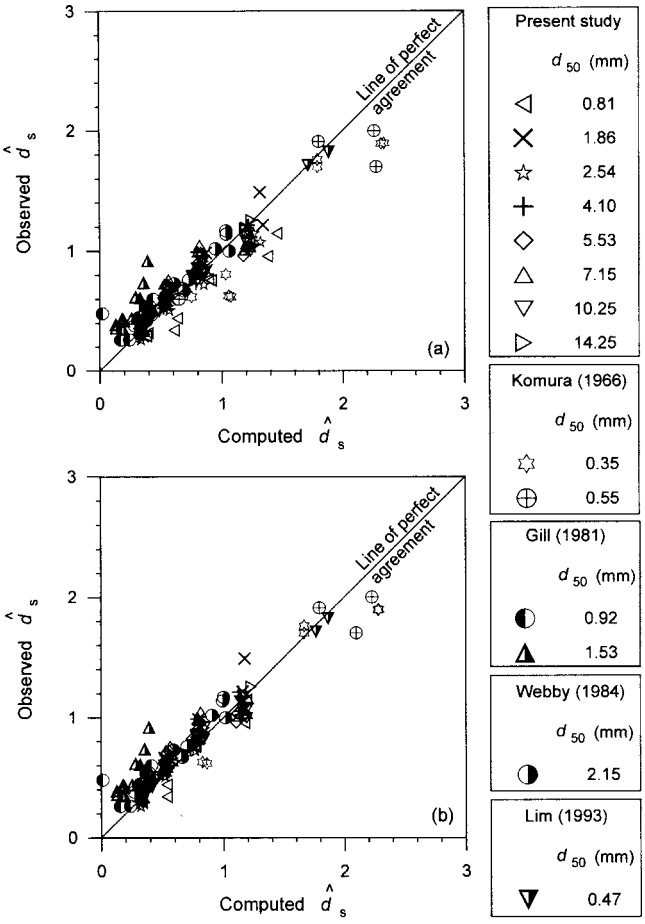

Fig. 5. (a) Comparison between the equilibrium scour depths $\hat{d}_s$ computed using clear-water scour model with sidewall correction and the experimental data and (b) comparison between the equilibrium scour depths $\hat{d}_s$ computed using clear-water scour model without sidewall correction and the experimental data

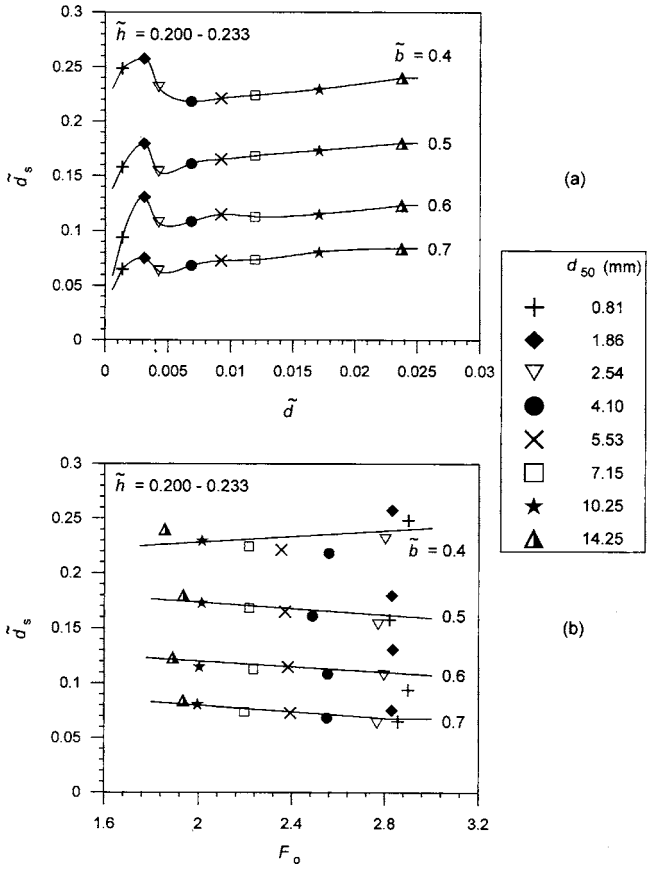

Fig. 6. (a) Variation of $\tilde{d}_s$ with $\tilde{d}$ for $\tilde{h}$=0.2–0.233 and different $\tilde{b}$ under $0.972 > U_1/U_c > 0.9$ and (b) variation of $\tilde{d}_s$ with F_0 for $\tilde{h}$=0.2–0.233 and different $\tilde{b}$ under $0.972 > U_1/U_c > 0.9$

($\tilde{d} \leqslant 0.0065$), $\tilde{d}_s$ increases up to $\tilde{d}$=0.003 and then decreases with $\tilde{d}$. However, in the curves, considerable hump followed by sag at the transition of sand and gravel exists. The probable reason is partly attributed to the fact that for sands, the formation of hump in the curves of $\tilde{d}_s$ versus $\tilde{d}$ is due to the transitional characteristics of the Shields diagram, where the bed shear stress required for the motion of sand particles is relatively less; and for gravels, the substantial increase of approaching flow velocity U_1 to maintain the condition of $U_1 \rightarrow U_c$ increases the bed shear stress within the contracted zone to a great extent, enhancing the scour potential that results in increase of $\tilde{d}_s$ at a constant rate.

Fig. 6(b) depicts the variation of nondimensional equilibrium scour depth $\tilde{d}_s$ with the densimetric Froude number F_0 for $\tilde{h}$=0.2–0.233 and different sediment sizes d_{50} under the approaching flow conditions of $0.972 > U_1/U_c > 0.9$. The scour depth $\tilde{d}_s$ gradually reduces with increase in the densimetric Froude number F_0 for larger opening ratios $0.5 \leqslant \tilde{b} \leqslant 0.7$. It indicates that the mobility of the sediment particles decreases with an increase in sediment size in relatively large opening ratios. However, for $\tilde{b}$=0.4, the trend is opposite due to the severity of contraction.

The laboratory experimental data (Table 2) for four channel opening ratios $\tilde{b}$, tested for different $\tilde{h}$ and median sediment diameters d_{50}=0.81–14.25 mm under the approaching flow conditions of $0.98 > U_1/U_c > 0.9$, are used to plot in Fig. 7(a) that shows the dependency of nondimensional equilibrium scour depth $\tilde{d}_s$ on $\tilde{h}$ for different $\tilde{b}$ and d_{50}. At lower $\tilde{h}$, nondimensional equilibrium scour depth $\tilde{d}_s$ increases significantly with an increase in $\tilde{h}$. The reason is attributed to the fact that the bed shear stress induced by the boundary layer within the contraction changes with approaching flow depth for lower $\tilde{h}$. However, as $\tilde{h}$ increases, $\tilde{d}_s$ becomes almost independent of $\tilde{h}$. For large opening ratio ($\tilde{b}$=0.7), scour depth $\tilde{d}_s$ is essentially independent of approaching flow depth at $\tilde{h}$=0.18, whereas for smaller $\tilde{b}$, the limit of independency of $\tilde{h}$ becomes approximately 0.23. This aspect may be justified that there is a little increase of bed shear stress as a result of fully developed boundary layer within the contracted zone due to increase in approaching flow depth beyond 0.18 and 0.23 times of the approaching channel width for larger ($\tilde{b} \geqslant 0.7$) and smaller ($\tilde{b} < 0.7$) opening ratios, respectively.

Fig. 7(b) presents the variation of nondimensional equilibrium scour depth $\tilde{d}_s$ with opening ratio $\tilde{b}$ for $\tilde{h}$=0.2–0.233 and different sediment sizes d_{50} under the approaching flow conditions of $0.972 > U_1/U_c > 0.9$. The scour depth $\tilde{d}_s$ significantly reduces with increase in opening ratio $\tilde{b}$. Because the reduction of flow

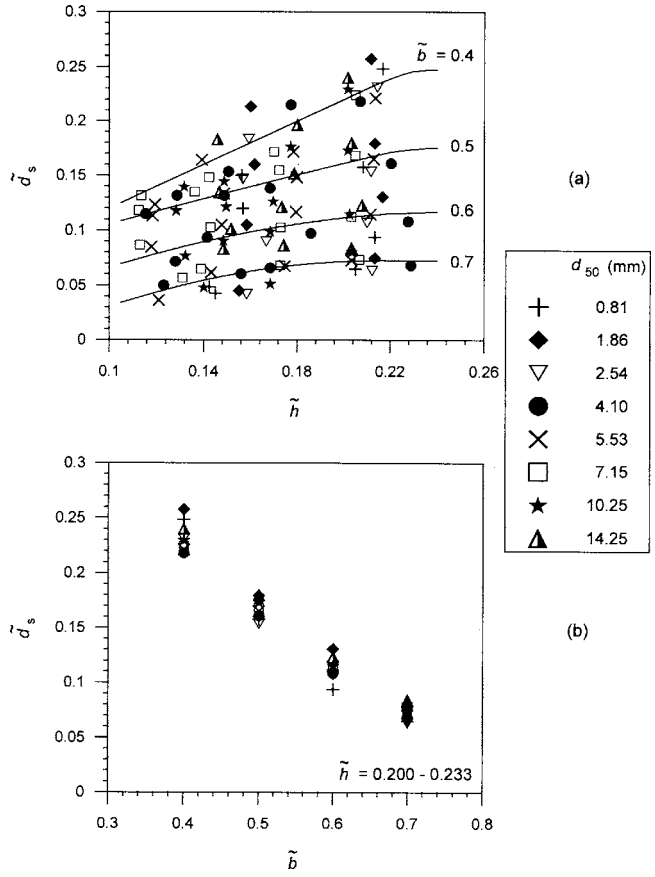

Fig. 7. (a) Variation of $\tilde{d}_s$ with $\tilde{h}$ for different $\tilde{b}$ and d_{50} under $0.98 > U_1/U_c > 0.9$ and (b) variation of $\tilde{d}_s$ with $\tilde{b}$ for $\tilde{h}=0.2-0.233$ and different d_{50} under $0.972 > U_1/U_c > 0.9$

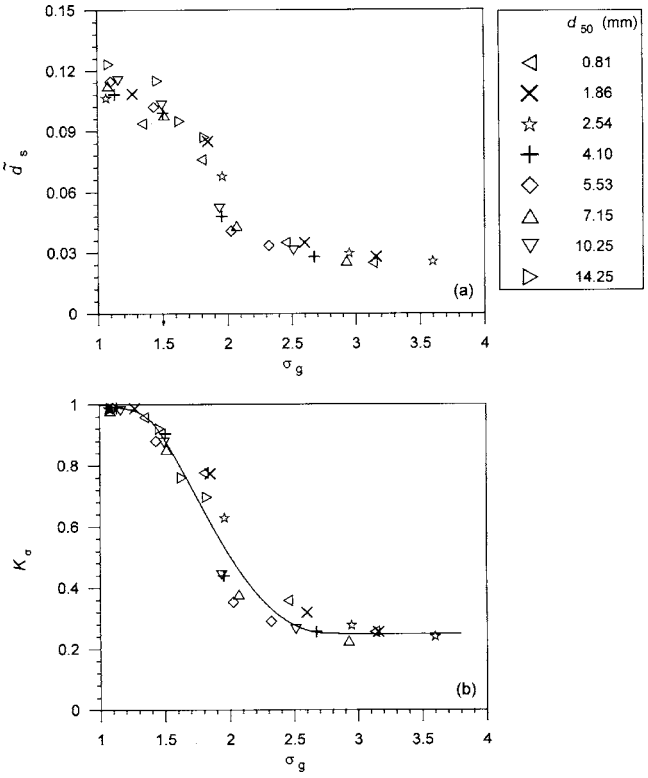

Fig. 8. (a) Dependency of $\tilde{d}_s$ on σ_g under $0.98 > U_1/U_c > 0.9$ and (b) coefficient K_σ as a function of σ_g under $0.98 > U_1/U_c > 0.9$

passage due to decrease of $\tilde{b}$ results in increase of flow velocity within the contracted zone, and thus bed shear stress increases to a great extent being capable to develop a greater magnitude of scour depth.

The laboratory experimental data (Table 3) for channel opening ratio $\tilde{b}=0.6$, tested for different gradations of nonuniform sediments under the approaching flow conditions of $0.98 > U_1/U_c > 0.9$, are used to plot Fig. 8(a) that presents the dependency of nondimensional equilibrium scour depth $\tilde{d}_s$ on geometric standard deviation σ_g of sediments. The particle size distribution has a pronounced influence on the scour depth. Nonuniform sediments ($\sigma_g > 1.4$) consistently produce lower scour depths than that in uniform sediments. The plots demonstrate a drastic decrease in scour depth that occurs for widely graded sediments. The equilibrium scour depth $d_s(\sigma_g)$ in nonuniform sediments can be estimated in terms of geometric standard deviation σ_g of sediments using the following relationship:

$$\tilde{d}_s(\sigma_g) = K_\sigma \tilde{d}_s \tag{4}$$

where K_σ=coefficient due to sediment gradation. The coefficient K_σ is defined as the ratio of equilibrium scour depth in nonuniform sediment ($\sigma_g > 1.4$) to that in uniform sediment. The variation of K_σ with σ_g is given in Fig. 8(b). It is apparent from the mean curve that the scour depth in nonuniform sediment with $\sigma_g=3$ is drastically reduced to 25% of scour depth in uniform sediment. However, the reduction of scour depth for $\sigma_g > 3$ is not influenced by the nonuniformity of sediments. In nonuniform sediments, a process of armoring in the scour hole commences resulting in an exposure of coarser particles due to washing out the finer fraction. The armor layer gradually increases the effective critical bed shear stress, which inhibits the development of scour hole. The mechanism of the formation of armor-layer within the scour hole is similar to the formation of secondary armoring in the scour hole at an abutment, as given in Dey and Barbhuiya (2004b).

Analytical Model

Energy and Continuity Equations

Applying the energy equation between Sections 1 and 2 for the flow situation at equilibrium scour condition (Fig. 1), one obtains

$$h_1 + \frac{U_1^2}{2g} = h_2 + \frac{U_2^2}{2g} - d_s + h_f \tag{5}$$

where h_f=head loss between Sections 1 and 2. Subscripts 1 and 2 refer to Sections 1 and 2, respectively. According to Graf (2003), if the reach of contraction is a long and gradual one, the resulting head loss h_f is negligible. The continuity equation between Sections 1 and 2 is

$$U_1 h_1 b_1 = U_2 h_2 b_2 \tag{6}$$

Determination of Scour Depth with Sidewall Correction

In clear-water scour, the equilibrium scour depth d_s reaches in a long contraction, when the flow velocity U_2 in the contracted zone becomes equaling critical velocity U_c for sediments. The

flow velocity $U_2|_{U_2=U_c}$ in the contracted zone can be determined from the well-known equation of bed shear stress as a function of dynamic pressure. It is

$$U_2|_{U_2=U_c} = u_{*c}\sqrt{\frac{8}{f_b}} \tag{7}$$

where f_b=friction factor associated with the bed. The Colebrook–White equation, used to evaluate f_b, is given as

$$\frac{1}{\sqrt{f_b}} = -0.86\ln\left(\frac{k_s P_b}{14.8A_b} + \frac{2.51}{R_b\sqrt{f_b}}\right) \tag{8}$$

where k_s=equivalent roughness height (=$2d_{50}$); A_b=flow area associated with the bed; P_b=the wetted perimeter associated with the bed (=b_2); and R_b=flow Reynolds number associated with the bed, that is $4U_2|_{U_2=U_c}A_b/(\nu P_b)$.

In the contracted zone, the bed is rough consisting of sediment particles and the sidewalls are smooth. Therefore, the friction factor associated with the wall f_w is considerably different from f_b. Therefore, Vanoni's (1975) method of sidewall correction is applied for the contracted zone of the channel, owing to the smooth wall and rough bed, as was done by Dey (2003a,b). Detailed derivation is available in Dey (2003a,b), where the solution for f_b was obtained from the following equations:

$$f_b = 0.316R_b\left(\frac{4U_2|_{U_2=U_c}A}{\nu P_w} - \frac{R_b P_b}{P_w}\right)^{-1.25} \tag{9}$$

$$\frac{1}{\sqrt{f_b}} = -0.86\ln\left(\frac{k_s U_2|_{U_2=U_c}}{3.7\nu R_b} + \frac{2.51}{R_b\sqrt{f_b}}\right) \tag{10}$$

where A=total flow area (=h_2b_2) and P_w=wetted perimeter associated with the wall (=$2h_2$). In clear-water scour, Eq. (6) becomes

$$U_1h_1b_1 = U_2|_{U_2=U_c}h_2b_2 \tag{11}$$

For a given data of U_1, h_1, b_1, b_2, and d_{50}, the unknowns $U_2|_{U_2=U_c}$, h_2, R_b, and f_b can be determined numerically solving Eqs. (7) and (9)–(11). Then, Eq. (5) is used to determine equilibrium scour depth d_s as given in

$$d_s = h_2 + \frac{U_2|^2_{U_2=U_c}}{2g} - h_1 - \frac{U_1^2}{2g} \tag{12}$$

The comparison of nondimensional equilibrium scour depths $\hat{d}_s$(=d_s/h_1) computed from the analysis with the clear-water scour experimental data (Tables 2 and 4) is shown in Fig. 5(a). The correlation coefficient being 0.94 indicates that the model fits excellently with the experimental data.

Determination of Scour Depth Without Sidewall Correction

This is a simplified approach, where the average flow velocity in the contracted zone $U_2|_{U_2=U_c}$ for equilibrium scour is determined using the equation of semilogarithmic average velocity as

$$\frac{U_2|_{U_2=U_c}}{u_{*c}} = 5.75\log\frac{h_2}{2d_{50}} + 6 \tag{13}$$

For a given data of U_1, h_1, b_1, b_2, and d_{50}, the unknowns $U_2|_{U_2=U_c}$ and h_2 can be obtained numerically solving Eqs. (11) and (13). Then, equilibrium scour depth d_s is determined from Eq. (12). The comparison of nondimensional equilibrium scour depths $\hat{d}_s$ computed from this method with the clear-water scour experimental data (Tables 2 and 4) is shown in Fig. 5(b). The correlation coefficient being 0.96 for the computed and the experimental data indicates that the model corresponds closely with the experimental data. This correlation coefficient is marginally higher than that for analysis with sidewall correction. The reason is that in calculation of scour depth with sidewall correction, many parameters are involved following a good number of iterations, as a result of which there is a possibility of more experimental scatter. Nevertheless, calculation of scour depth with sidewall correction is more methodical.

Maximum Equilibrium Scour Depth

Empirical Equation of Maximum Equilibrium Scour Depth

The parameters appropriate for the determination of equilibrium scour depth d_s in a long contraction has already been given in functional form in Eq. (2). The scour in a long contraction starts when the excess approaching flow velocity $U_{1e}(=U_1-U_1|^{d_s=0}_{U_2=U_c})$ is greater than zero. For no scour condition, U_{1e} is less than or equal to zero. Here, $U_1|^{d_s=0}_{U_2=U_c}$ refers to the approaching flow velocity U_1 that initiates scour in a long contraction. Therefore, $U_1|^{d_s=0}_{U_2=U_c}$ corresponds to U_1 for which U_2 becomes U_c for the undisturbed bed condition (d_s=0) in the contracted zone. The method of determination $U_1|^{d_s=0}_{U_2=U_c}$ is given in the Appendix. Hence, in Eq. (2), U_1 is replaced by U_{1e}. Also, to represent contraction scour equation, it is a usual practice to express nondimensional scour depth $\hat{d}_s$ as the ratio of scour depth d_s to approaching flow depth h_1. On the other hand, in preceding section of parametric study, scour depth d_s was normalized by b_1 in order to understand the real variation of d_s with various parameter, as b_1 is constant for a flume or channel (unlike h_1, which is a variable). Therefore, applying the same considerations (such as Δg, $\tilde{b}$ and negligible ν), as in the preceding section, and using the Buckingham π theorem with U_{1e} and h_1 as repeating variables, yields

$$\hat{d}_s = f_3(\mathsf{F}_{1e}, \hat{d}, \tilde{b}) \tag{14}$$

where $\mathsf{F}_{1e}=U_{1e}/(\Delta g h_1)^{0.5}$, that is the excess approaching flow Froude number; and $\hat{d}=d_{50}/h_1$. Eq. (14) is written for uniform sediments, as it does not include σ_g. However, for nonuniform sediments, the equilibrium scour depth $\hat{d}_s(\sigma_g)$ in long contractions can be estimated using coefficient K_σ for the corresponding value of σ_g [Fig. 8(b)].

The experimental data for $1 \geq U_1/U_c > 0.9$, given in Tables 2 (present experimental data) and 4 (data of other investigators), are used for the regression analysis, which yields the following equation of nondimensional equilibrium scour depth in long contractions:

$$\hat{d}_s = 0.368\mathsf{F}_{1e}^{0.55}\hat{d}^{-0.19}\tilde{b}^{-1.26} \tag{15}$$

The comparison of scour depths $\hat{d}_s$ estimated from the previous equation with the experimental data is shown in Fig. 9(a). The value of correlation coefficient between the computed and the experimentally obtained scour depths is 0.95. It indicates that the above equation fits well with the experimental data.

It is important to point out that there is always an inherent difficulty to run the experiments at the limiting condition of clear-water scour ($U_1=U_c$) with respect to the bed sediments in ap-

Table 4. Experimental Data of Different Investigators under Clear-Water Scour

Source	d_{50} (mm)	U_1 (m/s)	U_1/U_c	h_1 (m)	b_1 (m)	b_2 (m)	Observed d_s (m)	Computed with sidewall correction d_s (m)	Computed without sidewall correction d_s (m)
Komura (1966)	0.35	0.2468	1.000	0.0690	0.40	0.20	0.043*	0.074	0.059
	0.35	0.2475	0.985	0.0840	0.40	0.20	0.053*	0.088	0.069
	0.35	0.2444	0.974	0.0830	0.40	0.20	0.067*	0.086	0.067
	0.35	0.2046	0.834	0.0710	0.40	0.20	0.044	0.053	0.042
	0.35	0.1725	0.752	0.0450	0.40	0.10	0.079	0.080	0.075
	0.35	0.1725	0.752	0.0450	0.40	0.10	0.077	0.080	0.075
	0.35	0.2073	0.968	0.0290	0.40	0.10	0.055*	0.068	0.066
	0.35	0.2057	0.966	0.0280	0.40	0.10	0.053*	0.065	0.064
	0.55	0.2109	0.806	0.0570	0.40	0.20	0.034	0.037	0.031
	0.55	0.1932	0.800	0.0350	0.40	0.10	0.067	0.063	0.063
	0.55	0.2270	0.954	0.0320	0.40	0.10	0.064*	0.072	0.071
	0.55	0.2291	0.898	0.0470	0.40	0.20	0.080	0.107	0.099
Gill (1981)	0.92	0.3157	0.954	0.0686	0.76	0.50	0.032*	0.029	0.027
	0.92	0.2825	0.923	0.0436	0.76	0.50	0.024*	0.016	0.016
	0.92	0.3012	0.950	0.0533	0.76	0.50	0.029*	0.022	0.021
	0.92	0.3185	0.967	0.0668	0.76	0.50	0.040*	0.029	0.027
	0.92	0.2451	0.747	0.0655	0.76	0.50	0.017	0.011	0.010
	0.92	0.2411	0.805	0.0387	0.76	0.50	0.010	0.009	0.009
	0.92	0.2051	0.628	0.0637	0.76	0.50	0.031	0.001	0.001
	0.92	0.2454	0.875	0.0274	0.76	0.50	0.012	0.009	0.009
	1.53	0.3645	0.907	0.0543	0.76	0.50	0.040*	0.019	0.019
	1.53	0.3688	0.941	0.0476	0.76	0.50	0.044*	0.019	0.019
	1.53	0.3820	0.959	0.0518	0.76	0.50	0.028*	0.021	0.021
	1.53	0.3854	0.943	0.0591	0.76	0.50	0.029*	0.023	0.023
	1.53	0.2949	0.705	0.0671	0.76	0.50	0.024	0.009	0.009
	1.53	0.2987	0.704	0.0725	0.76	0.50	0.028	0.009	0.009
	1.53	0.3246	0.751	0.0805	0.76	0.50	0.035	0.015	0.014
	1.53	0.3649	0.844	0.0808	0.76	0.50	0.050	0.024	0.023
	1.53	0.3291	0.886	0.0363	0.76	0.50	0.012	0.012	0.012
	1.53	0.3121	0.754	0.0634	0.76	0.50	0.022	0.012	0.012
	1.53	0.3171	0.756	0.0683	0.76	0.50	0.029	0.013	0.013
	1.53	0.3477	0.817	0.0741	0.76	0.50	0.033	0.019	0.019
	1.53	0.3309	0.761	0.0835	0.76	0.50	0.035	0.016	0.016
	1.53	0.3752	0.878	0.0756	0.76	0.50	0.046	0.025	0.024
Webby (1984)	2.15	0.2378	0.431	0.1310	1.586	0.524	0.055	0.050	0.047
	2.15	0.3577	0.695	0.0885	1.586	0.524	0.104	0.091	0.088
	2.15	0.3672	0.694	0.1025	1.586	0.524	0.117	0.106	0.102
	2.15	0.2917	0.546	0.1085	1.586	0.524	0.075	0.073	0.071
	2.15	0.3728	0.705	0.1025	1.586	0.524	0.103	0.108	0.104
	2.15	0.3000	0.566	0.1040	1.586	0.524	0.079	0.075	0.073
	2.15	0.2690	0.517	0.0940	1.586	0.524	0.069	0.057	0.056
	2.15	0.3503	0.656	0.1080	1.586	0.524	0.110	0.102	0.098
	2.15	0.2706	0.500	0.1165	1.586	0.524	0.080	0.065	0.063
	2.15	0.2931	0.550	0.1065	1.586	0.524	0.071	0.073	0.071
	2.15	0.2133	0.392	0.1200	1.586	0.524	0.046	0.034	0.032
Lim (1993)	0.47	0.2083	0.960	0.0240	0.40	0.26	0.010*	0.010	0.010
	0.47	0.2231	1.000	0.0280	0.40	0.26	0.014*	0.014	0.013
	0.47	0.2083	0.960	0.0240	0.40	0.20	0.019*	0.018	0.019
	0.47	0.2232	1.000	0.0280	0.40	0.20	0.023*	0.024	0.023
	0.47	0.2083	0.960	0.0240	0.40	0.12	0.041*	0.041	0.042
	0.47	0.2232	1.000	0.0280	0.40	0.12	0.051*	0.053	0.052

Note: An asterisk (*) indicates scour data used for comparative study of existing scour equations and to develop Eqs. (15) and (16).

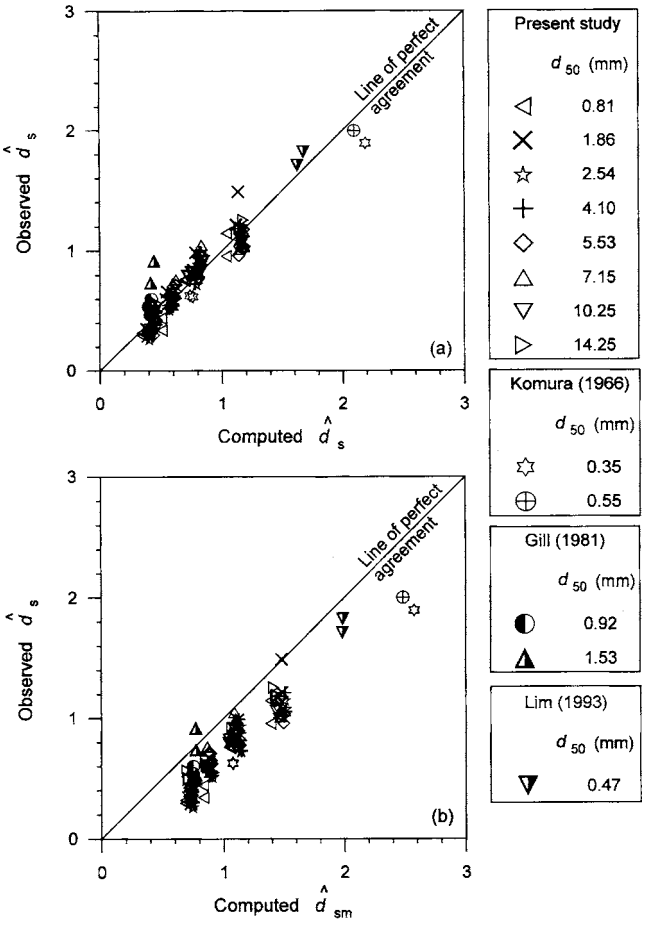

Fig. 9. (a) Comparison of the equilibrium scour depths $\hat{d}_s$ computed using Eq. (15) with the experimental data for $1 \geq U_1/U_c > 0.9$ and (b) comparison of the maximum equilibrium scour depths $\hat{d}_{sm}$ computed using Eq. (16) with the experimental data for $1 \geq U_1/U_c > 0.9$

proaching channel. This condition is recognized to be the most idealized condition of maximum equilibrium scour depth d_{sm} ($=d_s|_{U_1=U_c}$, that is the scour depth at $U_1=U_c$) in long contractions under clear-water scour (Gill 1981). It was observed that when the flow for an experimental run was set at $U_1=U_c$, there was a tendency to have a disturbed approaching channel bed. In order to avoid the problem, the experiments were conducted for the approaching flow condition being slightly less than U_c, that is $1 \geq U_1/U_c > 0.9$ (see Table 2). Therefore, to determine the equation of maximum equilibrium scour depth d_{sm} in long contractions, Eq. (15) is written for $U_1=U_c$. Thus, one gets

$$\hat{d}_{sm} = 0.368 \mathsf{F}_{1ec}^{0.55} \hat{d}^{-0.19} \tilde{b}^{-1.26} \tag{16}$$

where $\hat{d}_{sm}=d_{sm}/h_1$; $\mathsf{F}_{1ec}=U_{1ec}/(\Delta g h_1)^{0.5}$; and $U_{1ec}=U_1|_{U_1=U_c}-U_1|_{U_2=U_c}^{d_s=0}$. Eq. (16) is applicable for $0.66 \geq \mathsf{F}_{1ec} \geq 0.26$, $0.16 \geq \hat{d} \geq 0.0095$ and $0.7 \geq \tilde{b} \geq 0.4$. The experimental data for $1 \geq U_1/U_c > 0.9$, given in Tables 2 (present experimental data) and 4 (data of other investigators), are compared with the computed results using Eq. (16) as shown in Fig. 9(b). It is evident that Eq. (16) provides an adequate estimation of scour depth in long contractions, as most of the observed data lie below the line of perfect agreement. Eq. (16) also provides an economical estimation of scour depth, as it over predicts the experimental data within a reasonable limit (maximum 3.5 times the observed data).

Table 5. Equations of Maximum Equilibrium Scour Depth Proposed by Different Investigators

Investigator	Proposed equation
Laursen (1963)	$\hat{d}_{sm}+1=\tilde{b}^{-0.857}$
Komura (1966)	$\hat{d}_{sm}+1=1.6\mathsf{F}_{rc}^{0.2}\tilde{b}^{-0.67}\sigma_g^{-0.5}$, where F_{rc} is $U_1\|_{U_1=U_c}/(gh_1)^{0.5}$
Gill (1981)	$\hat{d}_{sm}+1=1.58\tilde{b}^{-0.857}$
Lim (1993)	$\hat{d}_{sm}+1=1.854\mathsf{F}_0^{0.75}\tilde{b}^{-0.75}\hat{d}^{0.25}$

Note: Equations of $\hat{d}_{sm}$ are expressed for $U_1/U_c \to 1$ or $u_{*1}/u_{*c} \to 1$. For uniform sediments, geometric standard deviation σ_g is considered to be unity.

Comparative Study of Different Predictors of Scour Depth

Phenomena involving local scour in long contractions have been studied most extensively in laboratory experiments, from which a number of empirical equations have been developed to estimate the maximum equilibrium scour depth (i.e., design scour depth) in long contractions. In general, they are based on a limited range of data. For example, scour data used for the derivation of empirical equations were mainly based on the approaching flow velocities U_1 being well below the critical velocities U_c for sediments. Moreover, scour of gravel beds in long contractions remains unexplored. As the maximum equilibrium scour depth d_{sm} in long contractions occurs at $U_1/U_c \to 1$ or $u_{*1}/u_{*c} \to 1$, the equations of maximum equilibrium scour depth proposed by different investigators can be written as given in Table 5. In these equations, the nondimensional scour depth is expressed as (d_{sm}/h_1+1). One of the reasons to express such nondimensional form is that the depression of the free surface at the contracted zone is insignificant in sand beds (flow Froude numbers ranging from 0.2 to 0.45). But, in gravel beds ($0.98 > U_1/U_c > 0.9$), a considerable depression of the free surface at the contracted zone was observed in the experiments (flow Froude numbers ranging from 0.7 to 0.85) (see Figs. 2 and 3). Therefore, it is convenient to express the nondimensional scour depth $\hat{d}_{sm}$ as the ratio of scour depth d_{sm} to approaching flow depth h_1.

The experimental data for $1 \geq U_1/U_c > 0.9$, given in Tables 2 (present experimental data) and 4 (data of other investigators), are used for the comparative study. The comparisons between the observed scour depths and computed scour depths using different existing equations are shown in Fig. 10. The equation proposed by Laursen (1963) underestimates observed scour depths to some extent being not safe for the design purpose, as a large number of data lie above the line of perfect agreement. It is important to mention that the predicting ability of the "maximum equilibrium scour depth d_{sm}" by Laursen (1963) shown in Fig. 10 should not be confused with Fig. 9(a), where best-fit equation of "equilibrium scour depth d_s" was derived. On the other hand, the equation of Gill (1981) is very conservative (uneconomical), as all the scour data lie well below the line of perfect agreement (maximum 6 times the observed data). The equations recommended by Komura (1966) and Lim (1993) provide a reasonable estimation of scour depth in long contractions, as they envelop almost all data and over predict less than Gill (1981) equation. However, it is

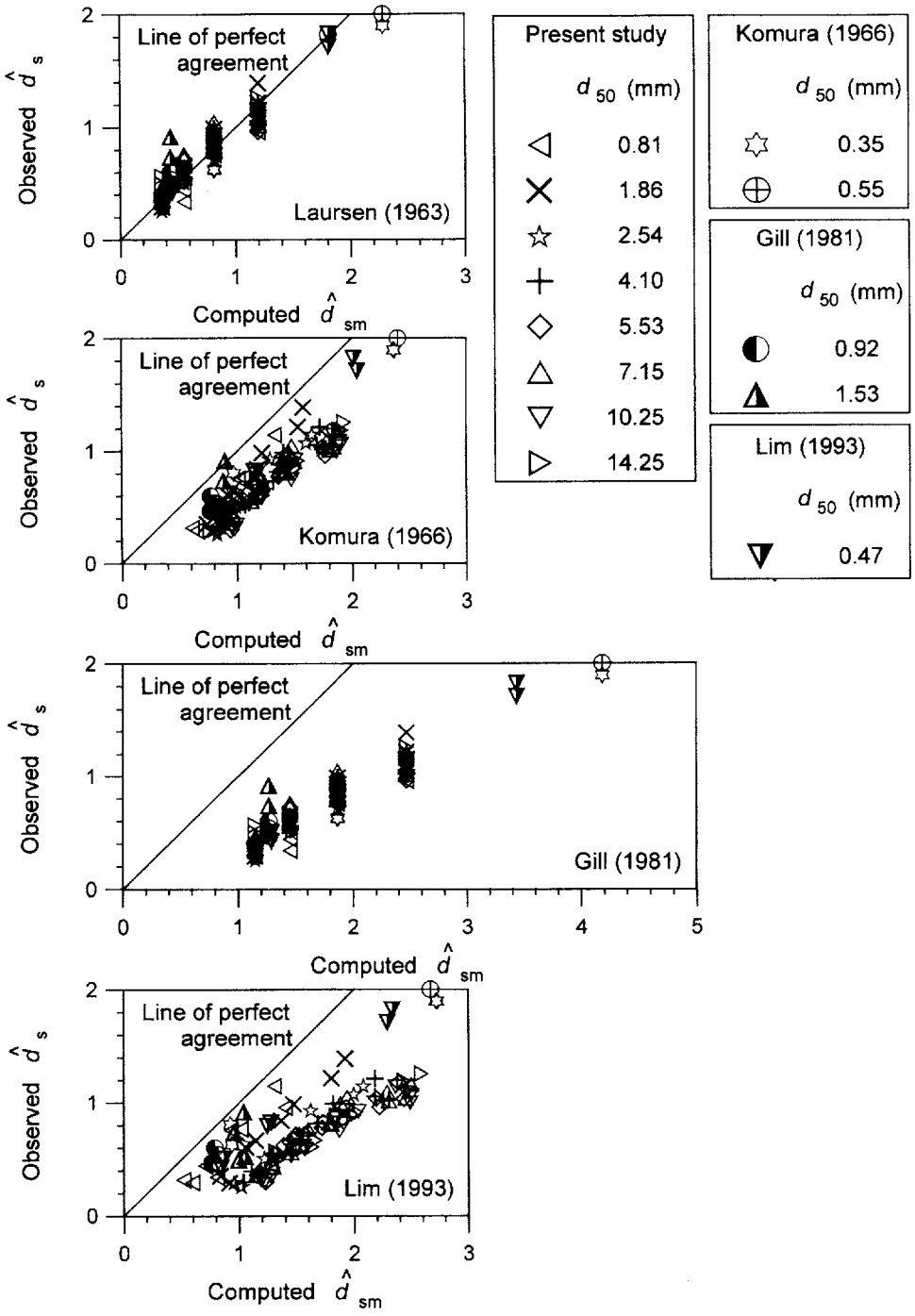

Fig. 10. Comparisons of the equations of maximum equilibrium scour depth $\hat{d}_{sm}$ proposed by different investigators with the experimental data for $1 \geq U_1/U_c > 0.9$

pertinent to point out that the four investigators used quite different sizes of sediments than that used in this study.

Conclusions

The findings of the investigation on local scour in long contractions for uniform and nonuniform sediments (gravels and sands) under clear-water scour are summarized as follows.

1. The scour depth increases with an increase in sediment size for gravels, but the curves of scour depth versus sediment size have considerable sag at the transition of sand and gravel.
2. The scour depth gradually reduces with an increase in the densimetric Froude number for larger opening ratios. However, for small opening ratios, the trend is opposite.
3. The scour depth increases with an increase in approaching flow depth at lower flow depths, but it becomes unaffected by the approaching flow depth at higher flow depths.
4. The scour depth increases with a decrease in contracted width of channel.
5. The nonuniform sediments reduce scour depth to a great ex-

tent due to the formation of the armor layer within the scour hole.

6. Based on the continuity and energy equations, a simple analytical model for the computation of clear-water scour depth in long contractions has been developed with and without sidewall correction for contracted zone. The scour depths computed using the models are in excellent agreement with the experimental data.
7. The characteristic parameters affecting the maximum equilibrium nondimensional scour depth (scour depth—approaching flow depth ratio), identified based on the physical reasoning and dimensional analysis, have been excess approaching flow Froude number, sediment size—approaching flow depth ratio, and channel opening ratio. The experimental data at the limiting stability of bed sediments in approaching channel under clear-water scour have been used to determine a new equation of maximum equilibrium scour depth through regression analysis.
8. Existing predictors for the maximum equilibrium scour depth have been compared with the experimental data. The comparison indicated that scour equations proposed by Komura (1966) and Lim (1993) are the best predictors among those compared, as they envelop almost all data and over predict within reasonable limit.

Appendix. Determination of Approaching Flow Velocity to Initiate Scour

Considering negligible head loss h_f and applying the energy equation between Sections 1 and 2 for bed sediments within contracted zone under critical (threshold) condition, that is $U_2=U_c$, before initiation of scour ($d_s=0$) (Fig. 1), the following equation is obtained:

$$h_1+\frac{\left(U_1\big|_{U_2=U_c}^{d_s=0}\right)^2}{2g}=h_2+\frac{\left(U_2\big|_{U_2=U_c}^{d_s=0}\right)^2}{2g} \tag{17}$$

The continuity equation between Sections 1 and 2 is

$$U_1\big|_{U_2=U_c}^{d_s=0}h_1b_1=U_2\big|_{U_2=U_c}^{d_s=0}h_2b_2 \tag{18}$$

The critical flow velocity at Section 2 can be determined using the equation of semilogarithmic average velocity as

$$\frac{U_2\big|_{U_2=U_c}^{d_s=0}}{u_{*c}}=5.75\log\frac{h_2}{2d_{50}}+6 \tag{19}$$

Therefore, for a given h_1, b_1, b_2, d_{50}, and u_{*c} (determined from the Shields diagram), the approaching flow velocity $U_1\big|_{U_2=U_c}^{d_s=0}$ required to initiate the sediment motion within the contracted zone can be estimated solving Eqs. (17)–(19) numerically.

Notation

The following symbols are used in this paper:

A = flow area [L^2];
A_b = flow area associated with bed [L^2];
b = channel width [L];
$\tilde{b}$ = channel opening ratio, that is b_2/b_1 [$M^0 L^0 T^0$];
$\tilde{d}$ = d_{50}/b_1 [$M^0 L^0 T^0$];
$\hat{d}$ = d_{50}/h_1 [$M^0 L^0 T^0$];
d_s = equilibrium scour depth [L];
$\tilde{d}_s$ = d_s/b_1 [$M^0 L^0 T^0$];
$\hat{d}_s$ = d_s/h_1 [$M^0 L^0 T^0$];
$\hat{d}_{sm}$ = d_{sm}/h_1 [$M^0 L^0 T^0$];
d_{sm} = maximum equilibrium scour depth [L];
d_{16} = 16% finer particle diameter [L];
d_{50} = median particle diameter [L];
d_{84} = 84% finer particle diameter [L];
F_{rc} = $U_1|_{U_1=U_c}/(gh_1)^{0.5}$ [$M^0 L^0 T^0$];
F_0 = densimetric Froude number, $U_1/(\Delta g d_{50})^{0.5}$ [$M^0 L^0 T^0$];
F_{1e} = excess approaching flow Froude number, $U_{1e}/(\Delta g h_1)^{0.5}$ [$M^0 L^0 T^0$];
F_{1ec} = excess approaching flow Froude number at $U_1|_{U_1=U_c}$, $U_{1ec}/(\Delta g h_1)^{0.5}$ [$M^0 L^0 T^0$];
f_b = friction factor associated with bed [$M^0 L^0 T^0$];
f_w = friction factor associated with wall [$M^0 L^0 T^0$];
g = gravitational acceleration [$L T^{-2}$];
h = flow depth [L] ;
$\tilde{h}$ = h_1/b_1 [$M^0 L^0 T^0$];
h_f = head loss [L] ;
K_σ = coefficient [$M^0 L^0 T^0$];
k = turbulent kinetic energy [$L^2 T^{-2}$];
$\hat{k}$ = k/U_1^2 [$M^0 L^0 T^0$];
k_s = equivalent roughness height [L] ;
L = length of contraction [L] ;
P_b = wetted perimeter associated with bed [L] ;
P_w = wetted perimeter associated with wall [L] ;
R_b = flow Reynolds number associated with bed [$M^0 L^0 T^0$];
s = relative density of sediments [$M^0 L^0 T^0$];
U_c = critical velocity for sediments [$L T^{-1}$];
U_1 = average flow velocity [$L T^{-1}$];
U_{1e} = excess approaching flow velocity [$L T^{-1}$];
U_{1ec} = excess approaching flow velocity corresponds to $U_1=U_c$[$L T^{-1}$];
u_* = shear velocity [$L T^{-1}$];
u_{*c} = critical shear velocity for sediments [$L T^{-1}$];
Δ = $s-1$[$M^0 L^0 T^0$];
η = z/b_1 [$M^0 L^0 T^0$];
ν = kinematic viscosity of water [$L^2 T^{-1}$];
ξ = x/b_1 [$M^0 L^0 T^0$].
ρ = mass density of water [$M L^{-3}$];
ρ_s = mass density of sediments [$M L^{-3}$];
σ_g = geometric standard deviation [$M^0 L^0 T^0$]; and
ϕ = angle of repose of sediments [$M^0 L^0 T^0$].

Subscripts

1 = section 1; and
2 = section 2.

References

Ashida, K. (1963). "Study on the stable channel through constrictions." *Annual Rep.*, Disaster Prevention Research Institute, Kyoto University, Kyoto, Japan, July, 312–327 (in Japanese).

Dey, S. (1997). "Local scour at piers, part 1: A review of development of research." *Int. J. Sediment Res.*, 12(2), 23–44.

Dey, S. (2003a). "Incipient motion of bivalve shells on sand beds under flowing water." *J. Eng. Mech.*, 129(2), 232–240.

Dey, S. (2003b). "Threshold of sediment motion on combined transverse

and longitudinal sloping beds." *J. Hydraul. Res.*, 41(4), 405–415.
Dey, S., and Barbhuiya, A. K. (2004a). "Clear water scour at abutments." *Proc. Inst. Civ. Eng., Water Management J.*, 157(June), 77–97.
Dey, S., and Barbhuiya, A. K. (2004b). "Clear-water scour at abutments in thinly armored beds." *J. Hydraul. Eng.*, 130(7), 622–634.
Dey, S., Bose, S. K., and Sastry, G. L. N. (1995). "Clear water scour at circular piers: a model." *J. Hydraul. Eng.*, 121(12), 869–876.
Dey, S., and Debnath, K. (2001). "Sediment pickup on streamwise sloping beds." *J. Irrig. Drain. Eng.*, 127(1), 39–43.
Gill, M. A. (1981). "Bed erosion in rectangular long contraction." *J. Hydraul. Div., Am. Soc. Civ. Eng.*, 107(3), 273–284.
Graf, W. H. (2003). *Fluvial hydraulics*, Wiley, Chichester, U.K.
Komura, S. (1966). "Equilibrium depth of scour in long constrictions." *J. Hydraul. Div., Am. Soc. Civ. Eng.*, 92(5), 17–38.
Lauchlan, C. S., and Melville, B. W. (2001). "Riprap protection at bridge piers." *J. Hydraul. Eng.*, 127(5), 412–418.
Laursen, E. M. (1963). "An analysis of relief bridge scour." *J. Hydraul. Div., Am. Soc. Civ. Eng.*, 89(3), 93–118.
Lim, S. Y. (1993). "Clear water scour in long contractions." *Proc. Inst. Civ. Eng., Waters. Maritime Energ.*, 101(June), 93–98.
Raikar, R. V. (2004). "Local and general scour of gravel beds." PhD thesis, Dept. of Civil Engineering, Indian Institute of Technology, Kharagpur, India.
Smith, C. D. (1967). "Simplified design for flume inlets." *J. Hydraul. Div., Am. Soc. Civ. Eng.*, 93(6), 25–34.
Straub, L. G. (1934). "Effect of channel contraction works upon regimen of movable bed streams." *Trans., Am. Geophys. Union*, (Part 2), 454–463.
Webby, M. G. (1984). "General scour at contraction." *RRU Bulletin 73*, National Roads Board, Bridge Design and Research Seminar, New Zealand, 109–118.
Vanoni, V. A. (1975). "Sedimentation engineering." *ASCE Manual No. 54*. ASCE, New York.
Yalin, M. S. (1977). *Mechanics of sediment transport*, Pergamon, New York.